JACS
JOURNAL OF THE AMERICAN CHEMICAL SOCIETY

ARTICLE

pubs.acs.org/JACS

Structural Fine-Tuning of a Multifunctional Cytochrome P450 Monooxygenase

Georg Zocher,[*,†,‡,#] Martin E. A. Richter,[§,#] Uwe Mueller,[‡] and Christian Hertweck[*,§,∥]

[†]Interfakultäres Institut für Biochemie, Eberhard Karls Universität Tübingen, Hoppe-Seyler-Str. 4, 72074 Tübingen, Germany
[‡]Helmholtz Zentrum for Materials and Energy Berlin, Macromolecular Crystallography Group, Albert-Einstein-Str. 15, D-12489 Berlin, Germany
[§]Leibniz Institute for Natural Product Research and Infection Biology (HKI), Beutenbergstr. 11a, 07745 Jena, Germany
[∥]Chair for Natural Product Chemistry, Friedrich Schiller University, Jena, Germany

Supporting Information

ABSTRACT: AurH is a unique cytochrome P450 monooxygenase catalyzing the stepwise formation of a homochiral oxygen heterocycle, a key structural and pharmacophoric component of the antibiotic aureothin. The exceptional enzymatic reaction involves a tandem oxygenation process including a regio- and stereospecific hydroxylation, followed by heterocyclization. For the structural and biochemical basis of this unparalleled sequence, four crystal structures of AurH variants in different conformational states and in complex with the P450 inhibitor ancymidol were solved, which represent the first structures of the CYP151A group. Structural data in conjunction with computational docking, site-directed mutagenesis, and chemical analyses unveiled a switch function when recognizing the two substrates, deoxyaureothin and the hydroxylated intermediate, thus allowing the second oxygenation-heterocyclization step. Furthermore, we were able to modify the chemo- and regioselectivity of AurH, yielding mutants that catalyze the regioselective six-electron transfer of a nonactivated methyl group to a carboxylic acid via hydroxyl and aldehyde intermediates.

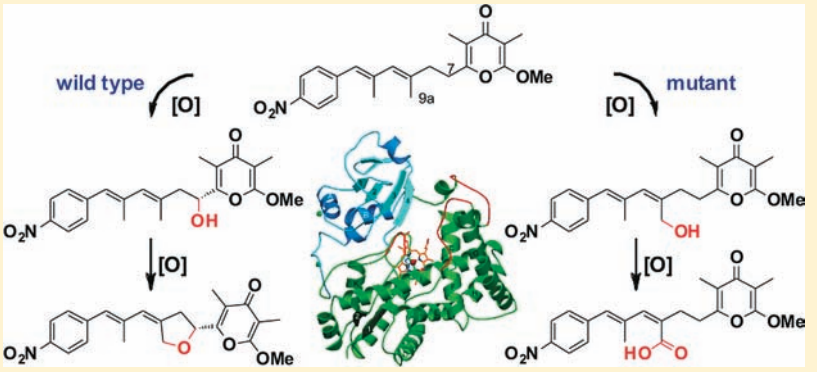

INTRODUCTION

Cytochrome P450 monooxygenases (P450s) are heme containing enzymes that play pivotal roles in catabolism and metabolism in all kingdoms of life.[1] In biosynthetic pathways, this group of enzymes has proven to be highly versatile not only with respect to the range of substrates, but also regarding the reactions catalyzed. These include C−C cleavage, heteroatom oxidation, as well as hydroxylation and epoxidation reactions,[2,3] which are often important tailoring reactions in terpene, alkaloid, and polyketide biosynthetic pathways. A hallmark of P450s involved in biosynthetic pathways is their high regio- and stereoselectivity, even when modifying nonactivated C−H groups.[4] Because these reactions are particularly difficult or even impossible to emulate with the currently available synthetic protocols, P450s have become highly valuable for biotechnological applications, in particular as biocatalysts[5] and biosensors.[6] During the past decades, a large body of knowledge on enzyme structures and the mechanism of P450-catalyzed oxygen transfer has been established.[2] However, it is remarkable that to date virtually all P450-catalyzed oxygen transfers are hydroxylations and epoxidations.[3] Multifunctional P450 monooxygenases are scarce, and there is an evident gap in knowledge on their structure and function. The full spectrum of P450-mediated oxygenation reactions clearly remains to be explored.

Recently, we have discovered an unusual multifunctional P450 monooxygenase, AurH from *Streptomyces thioluteus*, that is uniquely capable of forming a homochiral tetrahydrofuran ring.[7] This *O*-heterocycle is a vital component of the polyketide antibiotic aureothin (**1**, Scheme 1A),[8] as it lends rigidity to the carbon backbone and significantly contributes to the antifungal activity of the antibiotic.[9] *In vivo* and *in vitro* studies have revealed that AurH catalyzes an unprecedented tandem oxygenation process. First, AurH catalyzes an asymmetric hydroxylation of deoxyaureothin (**3**), yielding (7*R*)-7-hydroxydeoxyaureothin (**2**) as an intermediate, thus setting the absolute configuration of the final product (Scheme 1A). Second, AurH mediates another C−O bond formation that leads to *O*-heterocyclization.[10] AurH is capable of accepting a variety of pyrones as substrates, allowing for the first chemoenzymatic total synthesis of aureothin,[11] and

Received: November 11, 2010
Published: January 31, 2011

dx.doi.org/10.1021/ja110146z | *J. Am. Chem. Soc.* 2011, 133, 2292–2302

Scheme 1. (A) AurH Catalyzes Two Subsequent Oxidation Steps and Ring Formation from Deoxyaureothin (3) to Aureothin (1) via the Secondary Alcohol (7*R*)-7-Hydroxy-deoxyaureothin (2) and (B) Structure of the P450 Inhibitor Ancymidol

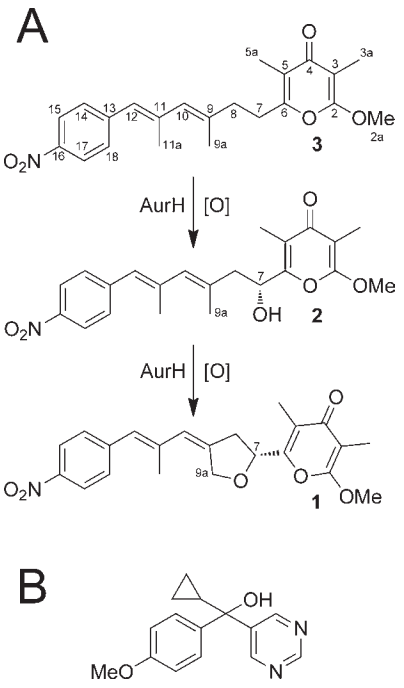

was also successfully employed in biotransformation reactions.[9] NorH, from the neoaureothin (spectinabilin) pathway, is a homologue of AurH and the only other known P450 enzyme catalyzing such an exceptional heterocyclization reaction.[12]

Here we report the first crystal structures of the multifunctional cytochrome P450 monooxygenase AurH. The structural data, in conjunction with inhibition studies, modeling, site-directed mutagenesis, and structure elucidation of novel metabolites, provide intriguing insights into the function of this fine-tuned biocatalyst. Furthermore, through protein engineering we succeeded in generating variants of AurH with altered function and regioselectivity, which led to the formation of a carboxylate branch in lieu of the THF ring.

RESULTS

Determination of the Structure of Cytochrome P450 Monooxygenase AurH. AurH was assigned to the cytochrome P450 superfamily by its P450 signature motif.[13] According to the CYP450 engineering database,[14] AurH is a member of the CYP151A family, which has not yet been structurally characterized. The protein, which consists of 406 amino acids, was overproduced in *E. coli* and purified to homogeneity.[10] A sample of pure AurH was crystallized, and its structure (nterm-AurH-II) was solved to 1.54 Å resolution by the use of multiwavelength anomalous diffraction (MAD) at the K-edge of iron (Table 1). Our initial construct of AurH revealed an *N*-terminal overhang of 10 amino acids, which was a remnant from the cloning and production strategy. This overhang swapped into a cleft above the entrance of the active center (see Supporting Information Figure S1A), and its impact on the structure of AurH was determined in another crystal form (nterm-AurH-I) with an unstructured *N*-terminal region that does not intersect the entrance of the active center (see Supporting Information Figure S1B). The structure of wild-type AurH (wt-AurH) was established at 2.1 Å resolution after reengineering the expression plasmid to avoid the *N*-terminal overhang. Finally, the structure of nterm-AurH-II in complex with the P450 inhibitor ancymidol (Scheme 1B; Ancy:AurH), a competitive inhibitor for P450s,[15] was determined at 2.3 Å resolution. Initial difference electron density maps clearly revealed the presence of the ligand in nterm-AurH-II and also showed that the *N*-terminal overhang formerly inserted into the cleft of the active center was removed by the soaking procedure. The structures of nterm-AurH-I, wt-AurH, and Ancy:AurH were determined by molecular replacement using nterm-AurH-II. Crystallographic refinement of all structures yielded models that possess low free *R*-factors, excellent stereochemistry, and small root-mean-square deviations (rmsd) from ideal values for bond lengths and bond angles (Table 2).

Overall Three-Dimensional Architecture of AurH and Structure Comparison. AurH is a monomeric protein and exhibits a typical prismlike cytochrome P450 fold with a length of about 60 Å and a thickness of about 35 Å. An AurH molecule consists of 15 helices (16 for nterm-AurH-II) and two β-sheets (Figure 1A). The overall structure and protein topology of AurH are similar to those of other P450 enzymes. A search for structural homologues using DALI[16] revealed that the closest structural relatives to AurH are PikC from pikromycin biosynthesis in *Streptomyces venezuelae*,[17] P450-SU1, whose native function in *Streptomyces griseoleus* is unknown,[18] *Bacillus subtilis* P450bioI, which plays a key role in biotin biosynthesis,[19] CalO2 from the calicheamycin biosynthetic pathway in *Micromonospora echinospora*,[20] StaP from staurosporin biosynthesis in *Streptomyces* sp. TP-A0274,[21] and P450epoK from epothilone biosynthesis in *Sorangium cellulosum* (see Supporting Information Table S1).[22] A closer inspection of these enzymes revealed conserved residues and regions crucial for cofactor binding and oxygen activation. Compared to the structural homologues, four regions of AurH showed significant Cα-rmsd deviations. These alternating positions are located at the substrate recognition sites (SRS)[23] and are composed of the *N*-terminal loop (amino acids 44 and 45), the FG-loop (amino acids 174 to 181), and the β2-loop (amino acids 389 to 394). Furthermore, compared to the structural homologues AurH varies at amino acids 66 to 91, which form a rigid two-helix bundle (helices B2 and B2′) and thereby create a hydrophobic wall that perfectly shields the active center from solvent. Other P450 proteins mainly exhibit random coil configurations with solvent-filled channels in this region. These solvent channels give rise to several possible entrance pathways as observed for a fatty acid hydroxylase from *Bacillus subtilis*.[24] In contrast, only a single entrance path exists in AurH because the two-helix bundle rigidly seals the active center. This substrate channel is classified as channel 2b based on the common notation of access pathways in P450 enzymes.[25] Besides AurH, such a two-helix bundle is only observed in CalO2.[20] However, compared to CalO2, the helices B2 and B2′ are kinked toward the *N*-terminal domain and thus yield an extended cavity. In general, the superimposition of the structural homologues described above revealed that AurH has a single substrate entrance leading to an elongated and wide cavity, which can perfectly harbor the substrate deoxyaureothin (**3**).

Comparison of the crystal structures of AurH disclosed that the largest deviations are located in mainly the same regions as described for the structural homologues. While nterm-AurH-I exhibits a closed setup, nterm-AurH-II revealed an artificially

Table 1. Data Collection Statistics[a]

			iron MAD of type nterm-AurH-II[c]					
	nterm-AurH-I[b]	nterm-AurH-II	peak	edge	hrem	lrem	Ancy: AurH	wt-AurH
beamline	BL 14.2	BL 14.2	BL 14.1	BL 14.1	BL 14.1	BL 14.1	BL 14.2	BL 14.2
wavelength (Å)	0.91841	0.91841	1.73844	1.74044	1.63138	1.85053	0.91841	0.91841
detector	marCCD 165	marCCD 165	marmosaic 225	marmosaic 225	marmosaic 225	marmosaic 225	marmosaic 225	marmosaic 225
resolution (Å)	30−2.30 (2.36−2.30)	20−1.54 (1.58−1.54)	20−2.05 (2.10−2.05)	20−2.07 (2.12−2.07)	20−1.92 (1.97−1.92)	20−1.99 (2.04−1.99)	25−2.30 (2.36−2.30)	25−2.05 (2.10−2.05)
spacegroup	$P2_12_12$	$H3$	$H3$	$H3$	$H3$	$H3$	$H3$	$C2$
no. measured reflns	196 705 (9566)	460 858 (19 367)	157 963 (11 292)	144 437 (10 437)	258 187 (18 449)	208 652 (14 643)	94 781 (6400)	210 711 (15 518)
no. unique reflns	38 128 (2707)	64 806 (4832)	56 821 (4219)	53 733 (3993)	69 578 (5138)	62 635 (4676)	19 673 (1428)	56 058 (4147)
R_{meas} (%)	11.7 (50.9)	4.0 (52.5)	5.9 (42.7)	7.1 (58.3)	6.1 (63.8)	6.1 (50.8)	10.1 (64.4)	13.9 (58.3)
completeness (%)	92.3 (90.2)	98.9 (99.3)	99.4 (99.7)	99.3 (99.9)	99.8 (100)	99.7 (99.8)	99.9 (99.4)	99.5 (99.6)
multiplicity	5.2 (3.5)	7.1 (4.0)	2.8 (2.7)	2.7 (2.6)	3.7 (3.6)	3.3 (3.1)	4.8 (4.5)	3.8 (3.7)
$\langle I\rangle/\langle\sigma(I)\rangle$	10.4 (2.7)	27.5 (2.9)	16.3 (2.9)	13.9 (2.8)	17.5 (2.5)	16.8 (2.8)	19.9 (2.6)	9.1 (2.7)
B-factor (Å^2)	33.9	28.4	30.8	31.9	30.8	30.6	28.9	25.4
mosaicity (deg)	0.38	0.19	0.25	0.25	0.25	0.25	0.31	0.19
subunit/ASU	2	1	1	1	1	1	1	2

[a] The unit cell parameters of nterm-II-AurH were a = b = 129.1 Å, c = 71.5 Å, for the high resolution data, and a = b = 129.5 Å, c = 72.7 Å, for the crystal used for the MAD experiment at K-edge of iron. For Ancy:AurH the cell parameter were a = b = 129.4 Å, c = 71.1 Å, and a = 152.4 Å, b = 54.1 Å, c = 130.3 Å, β = 123.3°, for the monoclinic spacegroup of wt-AurH. Values in parentheses are for the highest resolution shell. [b] Data set reveals the presence of pseudotranslational symmetry. [c] The Fe-peak wavelength was determined by X-ray fluorescence scans at the K-edge.

dx.doi.org/10.1021/ja110146z |J. Am. Chem. Soc. 2011, 133, 2292–2302

Table 2. Refinement Statistics

	nterm-AurH-I	nterm-AurH-II	Ancy:AurH	wt-AurH
resolution range (Å)	30−2.3	19.3−1.54	20−2.30	20.0−2.1
R_{cryst}	0.226	0.156	0.183	21.4
R_{free}	0.279	0.188	0.231	26.4
		Number of Non-H Atoms		
protein	3154/3171	3503	3193	3164/3164
heme	86	86	43	86
ancymidol			19	
chloride	2	3	3	5
sulfate	5	5		5
glycerol	18	12	12	
water	253	426	189	340
		Average Isotropic *B*-Factor (Å^2)		
main chain	27.0/32.2	29.8	31.7	27.9/22.7
side chain	27.6/32.8	32.4	32.0	29.5/24.8
heme	18.7/20.9	18.3	13.6	17.9/22.3
ancymidol			26.2	
chloride	58.6	37.5	37.6	40.4
glycerol	57.7	33.4	75.6	
water	26.2	26.8	23.5	28.4
rmsd for bond lengths (Å)	0.011	0.015	0.006	0.013
rmsd for bond angles (deg)	1.319	1.575	0.922	0.732
		Ramachandran Regions		
most favorable (%)	96.3	98.5	95.5	96.9
allowed (%)	3.2	1.5	3.2	2.8
outliers (%)	0.5	0.3	0.3	0.3

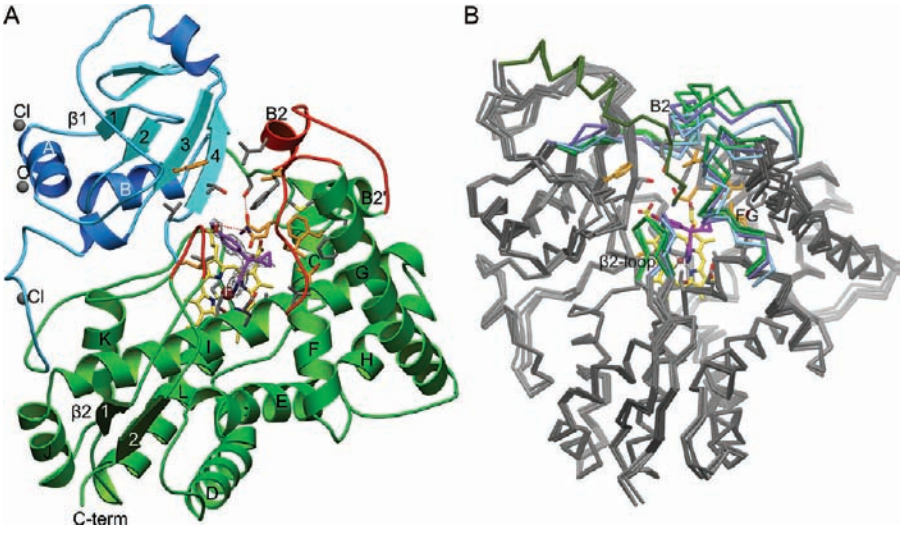

Figure 1. (A) Representation of Ancy:AurH exhibiting a typical prismlike shape of cytochrome P450 enzymes. The structure can be divided into a β-rich domain (blue) and an α-helical domain (green). Regions revealing the largest C_α-rmsd distances compared to nterm-AurH-I, nterm-AurH-II, and wt-AurH are highlighted in red. The inhibitor ancymidol, the heme, and several amino acids of the active center are shown in pink, yellow, and gray, respectively. Amino acids exchanged by site directed mutagenesis are ochre colored. (B) Superimposition of all AurH structures revealed that the differences are mainly located in the regions of substrate recognition. The flexible regions are emphasized by colors for Ancy:AurH (light green), nterm-AurH-II (dark green), nterm-AurH-I (light blue), and wt-AurH (violet).

wide opened state of the enzyme. The structures of Ancy:AurH and wt-AurH showed an intermediate conformation of both extremes but are related to nterm-AurH-II and nterm-AurH-I, respectively (Figure 1B). Differences between the two extrema, nterm-AurH-II (open state) and nterm-AurH-I (closed state), were observed at the two-helix bundle, where the tip of the two helix bundle (G76) is shifted by about 5.1 Å toward the active center. Furthermore, the FG-loop moves toward the same

dx.doi.org/10.1021/ja110146z |*J. Am. Chem. Soc.* 2011, 133, 2292–2302

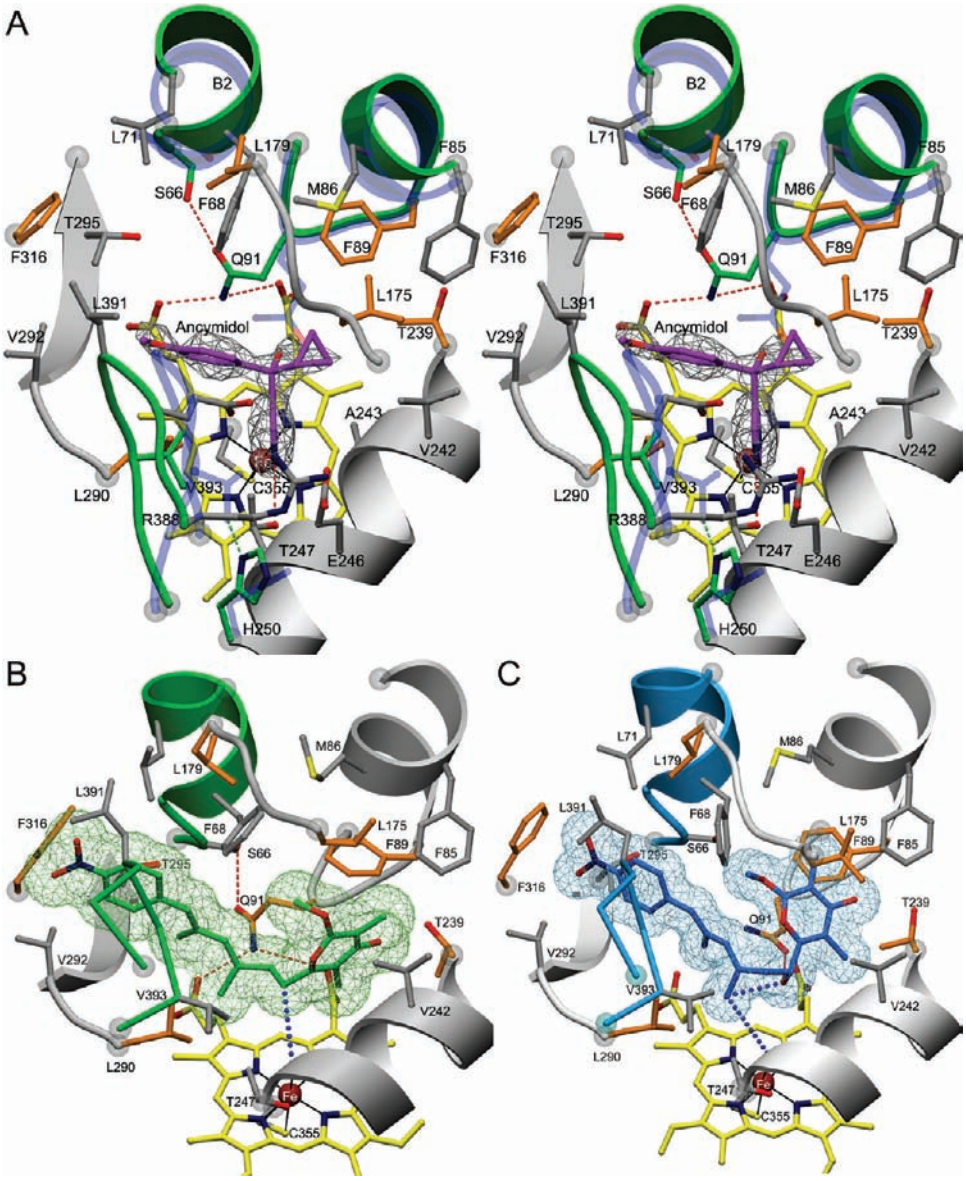

Figure 2. (A) Stereoview of the active center of nterm-AurH with ancymidol (magenta). Residues that were mutated to determine the influence on the catalytic reactivity are shown in green. The conformations of the Q91 and S66 in the unbound state (nterm-AurH-I in violet, Ancy:AurH in green) are highlighted by transparent ball-and-stick representation. The $(2F_o - F_c)$-omit map of ancymidol (gray) shown at an σ-level of 1.2 clearly defines the position of the inhibitor within the active center. (B, C) Proposed reaction pathway on the bases of *in silico* docking of the substrates **2** and **3** into the cavity of (B) nterm-AurH-II and (C) wt-AurH, repspectively, using AUTODOCK4.

direction, and the β2-loop is shifted by about 4 Å at G392 toward the FG-loop, which results in a weak main chain contact fixing the β2-loop in the closed setup. In this conformation, the entrance to the active center in wt-AurH and nterm-AurH-I is restricted. Investigation of the intermediate conformations of Ancy:AurH and wt-AurH indicated a subsequent closure of the two-helix bundle and disclosed the different conformation of the β2-loop, changing from an opened to a closed conformation.

Inhibitor Induces Conformational Changes at the Active Site. The active center of AurH is formed by the two-helix bundle that consists of B2 and B2′, the FG-loop, the I-helix, the loop between helix K and *N*-terminal β-sheet, and loop β2. The cavity of AurH is mainly formed by hydrophobic residues (Figure 2A), which is in agreement with the hydrophobic nature of the substrates (**2**, **3**). The inhibitor ancymidol is primarily bound through the interaction of the pyrimidine ring system to the heme iron and to the conserved residue T247. Other interactions to the inhibitor are mediated by loose and hydrophobic contacts (mainly to F89, A243, L175, L290, T295). This is also supported by the B-factor distribution of the inhibitor increasing from 20 Å^2 at the pyrimidine ring system to 52 Å^2 at the aromatic phenol moiety. The weak interaction of ancymidol is furthermore displayed by the low occupancy, which is refined to 75%. These observations reflect the low inhibitory effect of ancymidol on the *in vitro* activity of AurH and can be explained by the loose binding of the small inhibitor in a cavity, which is designed for the more voluminous substrates.

In comparison to the substrate free crystal forms of AurH, we found remarkable changes within the structure containing the

dx.doi.org/10.1021/ja110146z |*J. Am. Chem. Soc.* 2011, 133, 2292–2302

inhibitor ancymidol. First of all, binding of ancymidol is accompanied by a movement of the two helix bundle toward the closed state of the enzyme. Furthermore, inhibitor binding results in a reorientation of side chain Q91 toward the rigid wall of B2 and B2′. In one conformation, the amide function of Q91 is placed between the two negatively charged carboxy groups of the heme cofactor, thus presenting the hydrophobic carbon atoms of the side chain into the active center (Figure 2A). The reorientation of Q91 demonstrates flexibility of this residue during substrate binding. We concluded that Q91 plays a key role for catalysis and is able to adopt different conformations upon inhibitor binding, which results in presenting either the polar amide head or the hydrophobic carbons toward the active center. Notably, the glutamine residue is also present in NorH, which catalyzes an analogous reaction in the neoaureothin pathway. However, it is replaced in the structural homologues mainly by a hydrophobic residue. The importance of this position for catalysis is supported by structure comparison and site-directed mutagenesis. Structural comparisons revealed that hydrophobic residues, mainly leucine, replaced the polar glutamine in all homologous proteins depicted in Table S1. Furthermore, preparation of the Q91L mutant abolished catalysis completely. Moreover, reorientation of Q91 is accompanied by a flip of the carbonyl group of S66 toward the active center. As S66 is located at the *N*-terminal kink of the two-helix bundle and this reorientation of S66 is not observed in nterm-AurH-II nor in wt-AurH or nterm-AurH-I, we concluded that this movement is not a result from the removal of the *N*-terminal overhang and displays an inhibitor induced fit which occurs during substrate binding.

Second, a detailed comparison of the active centers of Ancy:AurH with the unbound states of AurH revealed an inhibitor-induced incorporation of an additional water molecule into the cleft of helix I, which is crucial for the catalytic process and proton transfer. The incorporation of additional water molecules into the groove of the I-helix during binding of molecular oxygen was described for P450Cam.[26,27] The incorporation of these active site water molecules is accompanied by a "flip" of the acidic carbonyl oxygen, which widens the helix. Although this reorganization is not observed in Ancy:AurH, the hydroxy group of T247 is pushed outward to form a hydrogen bond to the nitrogen atom of the inhibitor. In comparison to conformational changes induced by inhibitor binding of ketoconazole as described for P450eryF,[28] the cleft in helix I remains stable and did not collapse upon inhibitor accumulation. However, incorporation of the water molecule and the rotation of T247 toward ancymidol pushed the conserved residues E246 and T247 upward by about 0.5 Å away from the heme cofactor. This results in a rotation of the adjacent aromatic side chain of H250 by about 50° and is accompanied by the loss of the hydrogen bond network, which connects helix I with loop β2 (Figure 2A). As a consequence, loop β2 swings out by about 4 Å to avoid a steric clash of the rigid imidazol ring system of H250 with the branched side chain of V393. This enables tension of the loop β2 and opens the reaction center. We assume that this tension might be important for catalysis as our docking calculations revealed that the pressure of loop β2 is able to bend the substrate and facilitates a geometry that presses the substrate deeper into the pocket and pushes atom C-9a toward the reaction center. A comparable hydrogen bond network connecting loop β2 with helix I is found in P450SU-1 from *S. griseoleus*, which bis-hydroxylates vitamin D3.[18] Yet, a substrate-induced fit of this region during substrate incorporation has not been observed. Nevertheless, it is well conceivable that the relaxation of loop β2 is essential for THF ring formation in transferring the tension of this loop to the intermediate, which bends the rigid unsaturated part of (7*R*)-7-hydroxydeoxyaureothin (**2**) (Figure 2A). Interestingly, the hydrogen bond network of D397-H230-E246 is conserved in NorH, thus pointing to a crucial catalytic function of the flexible β2-loop.

Substrate Modeling Illuminates Stereochemical Course of Oxygenation and Unveils Switch Function of AurH. As attempts to incorporate the natural substrates of AurH into the crystal have not been successful, we performed a computational docking of the substrates (**2**) and (**3**) on structures of Ancy:AurH, wt-AurH, and nterm-AurH-I. These dockings resulted in models for both oxidative reactions and elucidate the crucial role of Q91, which adopts different conformations depending on the actual substrate. *In silico* docking of the substrate deoxyaureothin (**3**) into the cavity of nterm-AurH-I using the Lamarckian genetic algorithm implemented in AUTODOCK4[29] provides a model for the first step of the oxidative enzymatic reaction and perfectly rationalizes its regioselectivity and stereospecificity in forming the hydroxyl intermediate (Figure 2B). The elongated substrate fits snugly into the active center. Our model revealed contacts between the substrate and residues F19, F68, Q91, V292, T295, L290, F316, L391, and G392. The pyrone ring of the substrate occupies a hydrophobic pocket built by F85, F89, L175, V242, A243, and T239. By comparison of structurally homologous P450s in the substrate bound state, we found that this portion of the cavity is occupied frequently, as has been observed for P450bioI,[19] StaP,[21] P450epoK,[22] PikC,[17] and P450-SU1.[18] According to our model, the substrate adopts an orientation where C-7 and the reactive oxygen species at the heme iron have a distance of about 4.0 Å. Locked in this conformation, the substrate is attacked from the Resite, which is in full accord with the observed 7*R* configuration of the product. Moreover, Q91 adopts a conformation in analogy to the scenario observed in Ancy:AurH and presents the hydrophobic carbon atoms toward the educt while potentially forming a hydrogen bond to the carboxy group of the cofactor. As described above, this might trigger an educt-induced fit of the active center. In docking experiments using wt-AurH, which exhibits a wider cavity, (7*R*)-7-hydroxydeoxyaureothin (**2**) is able to adopt a conformation that allows THF ring formation during the second oxidative reaction step (Figure 2C). This model reveals a hydrogen bond between the secondary alcohol and Q91, the side chain of which retains its conformation and exerts steric pressure on the intermediate toward the iron. As a result, the calculated distance of C-9a to the distal heme water, which is approximately in the position of the activated oxygen species, is about 4.7 Å. Formation of the THF ring becomes possible because the 7-hydroxyl group is oriented in a geometry enabling an intramolecular back-side attack of an activated C-9a. The cavity of AurH remains in a closed conformation as steric pressure is required to bend the rigid unsaturated intermediate. Nevertheless, compared to nterm-AurH-I, the cavity of wt-AurH is still wider due to the relaxed state of the two-helix bundle. This is a reasonable observation because the substrate is bulkier when bent and explains why such a conformation is not found by *in silico* modeling into the tight cavity of nterm-AurH-I. Furthermore, steric pressure exerted by loop β2 seems to be essential in both oxidative steps, as docking calculations in Ancy:AurH reveal a degree of flexibility of the substrate in the cavity, which is not observed in nterm-AurH-I and wt-AurH. However, most of these conformations can be neglected as they are inconclusive with the observed

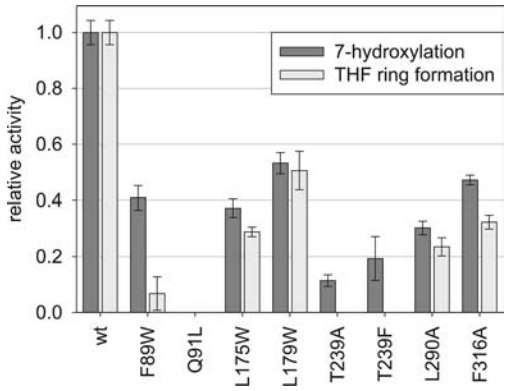

Figure 3. Relative activity of AurH mutants, comprising contents of the two sequential products, (**2**) (7*R*)-7-hydroxydeoxyaureothin and (**1**) aureothin.

stereoselectivity and the regioselectivity of the enzyme and are not supported by our mutagenesis experiments.

Finally, our docking calculations are supported by the finding that a conversion of the α-pyrone derivative of **3**, iso-deoxyaureothin, into iso-aureothin is not observed, whereas iso-deoxyaureothin is hydroxylated at C-7 and formation of the THF ring does not take place.[9] This is reasonable as steric collision of iso-deoxyaureothin with the pyrone binding pocket (residues T239 and F89) can easily be avoided by a 180° rotation of the pyrone ring system compared to deoxyaureothin during the initial hydroxylation step. Such a rotation excludes the geometry required for THF ring formation, as this orientation would force an intramolecular clash of the atoms C-5a and C-10 of iso-deoxyaureothin when adopting the calculated conformation needed for the second oxidation. Furthermore, we calculated a model for NorH using MODELLER[30] on the basis of wt-AurH and compared regions exhibiting sequence differences around the active center. Apart from the catalytic residue E246, which is replaced by a glutamine residue in NorH, the models only differ in regions involved in binding of the hydrophobic tail and the aromatic system of neoaureothin. This clearly supports a correct docking as differences in the protein sequence are observed in regions where our substrate models differ from neoaureothin. Point mutations F19I, L71V, L290T, P291T, L391T, and F316W would rebuild the cavity of AurH to the wider cavity of NorH, which fits the extended backbone of neoaureothin.

Site-Directed Mutagenesis Supports the Model for Substrate Binding and Reaction Mechanism. To provide experimental support for the calculated models, we performed site-directed mutagenesis of several amino acids predicted to be involved in substrate binding. Next, we determined the activity of the mutated enzymes compared to the wild type by adding deoxyaureothin (**3**) to cultures of *Streptomyces albus* strains expressing mutated *aurH* variants (Figure 3). The catalytic importance of Q91 is emphasized by site-directed mutagenesis to leucine, which completely abolishes enzymatic activity for the first reaction step. This was expected because the initial oxygenation reaction is hindered by the branching methyl group at the γ-carbon atom of leucine. Furthermore, the educt-induced fit of the rigid two-helix bundle is hampered because leucine is not able to adopt the conformation toward the carboxy groups of the cofactor observed in Ancy:AurH. The conversion of intermediate (**2**) by the Q91L mutant to aureothin (**1**) is also abolished (data not shown), which supports our docking model. The more voluminous

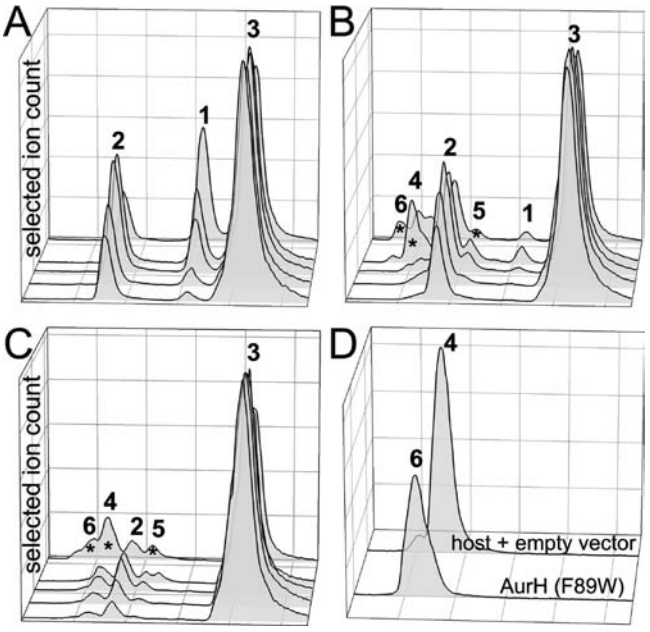

Figure 4. Selected *in vivo* biotransformations of deoxyaureothin (**3**) by (A) AurH wild type, (B) F89W mutant, and (C) T239F mutant. Time course (front to back): 15, 45 min, 2, 4, 24 h. (D) Biotransformation of 9a-hydroxydeoxyaureothin (**4**) to the carboxylic acid **6** by AurH(F89W) over 24 h.

side chains introduced by the mutants L175W and L179W decreased the catalytic activity for both oxygenation reactions, which is an effect of steric collision. As expected, the mutation of L290 to alanine led to a decrease in substrate conversion because L290 forms a tight hydrophobic contact in both oxidative reaction models. The loss in activity of F316A clearly indicates the participation in substrate binding. The decreased turnover of F316A is expected from our docking model as the nitro entity of the substrate would interact with the aromatic system of F316 to yield a close hydrophobic contact. To corroborate the correct modeling of the pyrone ring portion of the substrate, we exchanged F89 to tryptophane and T239 to alanine and phenylalanine, respectively. All three mutations significantly decreased enzymatic performance. Although a minimal conversion to the intermediate was observed, no ring formation occurred when T239 was altered. While the activity of T239A clearly supports participation of T239 in a hydrogen bond to the intermediate during catalysis, an exchange to phenylalanine avoids this stabilizing effect and furthermore decreases the transformation rate by steric pressure. Interestingly, the ring formation of the mutant F89W is almost completely lost, while C-7 hydroxylation is still observed at reasonable rates. As the phenyl moiety of F89 directly contacts the pyrone entity (Figure 2B, C) one may conclude that the turnover of the intermediate is impaired by steric collision. Furthermore, the increased size of W89 pushes the pyrone ring system toward loop β2 and does not allow the intermediate to adopt the geometry that is required for a backside attack of the C-7 hydroxyl to C-9a. As a consequence, THF ring formation has become highly unfavorable.

Engineering of an AurH Variant Catalyzing a Six-Electron Oxidation. Among the various engineered mutants, we noted that two AurH variants containing altered residues that interact with the pyrone ring transformed **3** into new aureothin derivatives (Figure 4A−C). From chromatographic profiles, UV absorption,

Scheme 2. AurH Mutants Catalyze the Sequential C-9a Oxygenation of 3 with Structures of New Aureothin Analogues 4−6

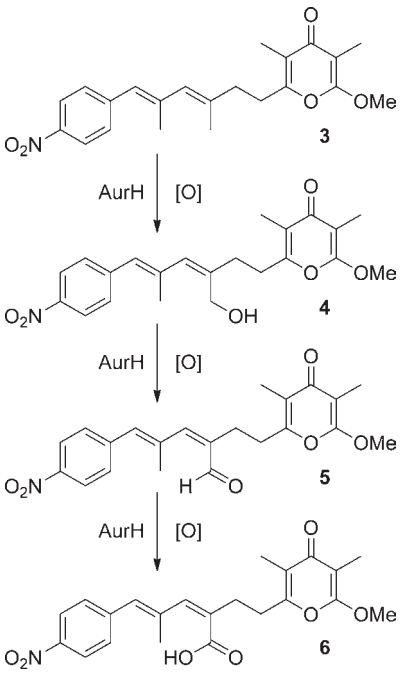

and MS of the products, these mutants obviously catalyzed aberrant oxygenation reactions. To elucidate these, a full structural determination of the new derivatives was needed. Since the amounts obtained in the *in vitro* assay were too low, we complemented a *Streptomyces albus* host harboring the *aur* biosynthesis gene cluster except for *aurH* (knockout mutant) with *aurH* constructs coding for the AurH(F89W) and AurH(T239F) variants, respectively. Cultivation of these *S. albus* strains afforded sufficient material for a full characterization by 1D and 2D NMR spectroscopy. Analyses of the NMR data revealed the structures of the new metabolites (**4**−**6**). Interestingly, all new compounds represent deoxyaureothin derivatives oxygenated at C-9a, differing only in the degree of oxidation (Scheme 2). This fact is well depicted by the proton and carbon NMR signals at this position. While the signals corresponding to the methylene group at C-7, the place of hydroxylation of native AurH, remain almost constant with ascending degree of C-9a oxygenation (see Supporting Information Table S2), the singlet at 1.96 ppm, which corresponds to three methyl protons at C-9a in deoxyaureothin (**3**) changes to a singlet at 4.22 ppm (relative intensity of two protons) in 9a-hydroxydeoxyaureothin (**4**), a singlet at 9.48 ppm (one proton) in deoxyaureothin-9a-aldehyde (**5**), and a broad signal at 12.9 ppm (one proton) in deoxyaureothin-9-carboxylic acid (**6**), respectively. Carbon NMR signals support the identities of the functional groups (18.1, 64.9, 194.9, and 170.3 ppm for methyl, hydroxyl, aldehyde, and carboxylic acid group, respectively). Interestingly, while the mutated enzymes were still able to hydroxylate C-7, no derivatives resulting from oxygenation at both C-7 and C-9a were detected. Apparently, products that are oxygenated at C-9a cannot bind to the engineered enzyme in a manner that would allow for C-7-oxygenation and vice versa. Finally, through the successful biotransformation of pure **4** into **6**, we proved that the oxygenation of the alcohol to the acid is indeed catalyzed by AurH variants (Figure 4D).

DISCUSSION

In this study, we have elucidated the structure and function of the unique multifunctional P450 monooxygenase AurH that sequentially installs two C−O bonds into the aureothin polyketide backbone to yield a homochiral THF ring. We obtained AurH in four distinct crystallized forms, with one containing the bound inhibitor ancymidol. These isoforms illustrate the transition from "open" to "closed" enzyme conformations. Overall, the AurH structure exhibits a typical P450 fold. However, the two-helix-bundle (B2, B2′), which shields the active center from solvent, is uncommon and was only reported for CalO2.[20] When AurH changes from "open" to "closed" conformation, the two-helix-bundle and the FG-loop move toward the active center, and the β2-loop approaches the FG-loop. Altogether, this seems to generate steric pressure not only to push the substrate into the correct position, but also to bend the carbon backbone, thus facilitating THF-ring formation. The residue at the *N*-terminal kink of the two-helix-bundle (S66) moves upon inhibitor binding and Q91 turns toward the heme group. A plausible scenario would involve an induced-fit mechanism triggered by substrate binding. Disintegration of protein crystals in soaking experiments with substrates implies substantial movements upon substrate binding and catalysis.

Another unique feature of AurH is the S66-Q91 pair, which is not found in similar P450s, except for the homologue NorH from the neoaureothin pathway. Docking studies imply a switch function in recognizing the two substrates, deoxyaureothin (**2**) and the hydroxylated intermediate (**3**). The abolished activity in the Q91L mutant points to an important role of Q91 in enzyme function and/or structure.

Our *in silico* docking calculations were complemented and fully supported by a series of site-directed mutagenesis experiments. The activities of the mutants were determined *in vivo* and compared to the wild type. Although the reaction was remarkably slower *in vivo* (50% substrate conversion not reached after 24 h) than *in vitro* using wild type enzyme (50% conversion in about eight hours[10]), this setup allowed for a quick and parallel investigation of substrate conversion. This is not surprising as one should take into account that the *in vivo* enzyme concentration does not reach such high values as 5 μmol L^{-1} *in vitro*. However, results from our comparative studies with wild type and mutants clearly support the hypothesis that narrowing the cavity for pyrone binding prevents the substrate from adopting the correct steric conformation for THF ring formation, although the initial hydroxylation is still possible to some degree. This is reasonable, because bending the substrate to obtain correct geometry for THF ring formation results in a bulkier reactant, and formation of the heterocycle is excessively sensitive because of this steric pressure.

Interestingly, the two successive substrate binding modes observed for AurH are clearly distinct from other known multifunctional P450s. For PikC, two different desosamine anchoring sites have been identified that allow for the recognition of two different substrates.[17] P450BioI positions the fatty acid substrate in a U-shaped conformation that brings both carbon atoms in position for consecutive hydroxylation and oxidative C−C-bond cleavage.[19] In contrast to AurH, a conformational change of the substrate between the first and the second reaction has not been observed.

The crystal structures and mutagenesis studies indicate that the substrate is directed to the active site mostly by hydrophobic interactions and π-stacking. Altering these residues (L175W,

L179W, L290A, F316A) decreased the overall activity but had no influence on regioselectivity or THF-ring formation. As it is known from other P450s, for instance mammalian CYPs[31] or PikC,[32] hydrophobic interactions are mostly nonspecific. Yet, for correct substrate positioning and selectivity, polar residues that specifically recognize corresponding substrate functionalities are more important, which is well supported by the drastically impaired activity of Q91 and T239 mutants.

In addition to substantiating our structure and modeling studies, the mutagenesis experiments yielded AurH variants with an altered function. While some mutants solely lost the ability to produce an *O*-heterocycle, two mutants (F89W and T239F) exhibited a change in regioselectivity. While the wild type invariably hydroxylates C-7 in the first step, the mutants were capable of C-9a hydroxylation. Furthermore, the AurH variants catalyzed multiple rounds of oxygenation, which resulted in the formation of the C-9a aldehyde and carboxylate derivatives. Recent examples for altered substrate specificity and regioselectivity of mutated P450s include human CYP2A6, mutants of which were able to oxidize substituted indoles[33] and *B. megaterium* P450BM3 with altered substrate specificity[34,35] or increased activity,[36] and *B. subtilis* CYP102A3, which was evolved to a higher selectivity for hydroxylation of terminal carbon atoms of octane.[37] In a similar fashion, the regioselectivity of PikC was changed upon mutagenesis.[17] Oxidation of YC-17 at different positions yielded methymycin and neomethymycin in equivalent amounts, whereas mutant E85Q preferentially formed methymycin, which again highlights the importance of hydrophilic residues for substrate positioning. In comparison, AurH catalyzes the regioselective oxidation at two distinct positions. However, in stark contrast to PikC, the reaction follows a sequential manner. In the F89W and T239F mutants, the reaction sequence was disturbed. Due to steric pressure, anchoring of the pyrone entity requires an alternative binding mode, which does not allow the binding of a C-7 hydroxylated product and oxidation at position C-9a and vice versa. This is plausible as the flexibility of loop β2 would allow antagonizing the steric hindrance of the bulky side chains of the mutants.

Apart from the altered regioselectivity, the AurH mutants stand out because of their ability to catalyze the stepwise oxygenation of the C-9a methyl group to a carboxyl moiety. Despite extensive research on P450s, it is surprising that to date only a handful of P450s are known that catalyze similarly the full oxidation of methyl groups to carboxylic acids in biosynthetic pathways. These rare P450s include ent-kaurene-oxidase and P450−1 in gibberellic acid (GA) biosynthesis in *Arabidopsis thaliana*[38] and *Gibberella fujikuroi*,[39] respectively, abietadienol/abietadienal oxidase PtAO in resin acid biosynthesis in conifers,[40] and CYP71AV1 from *Artemisia annua* that transforms amorpha-4,11-diene to artemisinic acid.[41] The multifunctional P450 BorI from borrelidin biosynthesis in *Streptomyces parvulus* Tü4055 is also capable of oxidizing a methyl group to an aldehyde, which may be further oxidized to the carboxylic acid in a shunt pathway.[42] However, to the best of our knowledge the change of function from sequential hydroxylation/heterocyclization to a full six-electron oxidation of a nonactivated methyl group is fully unprecedented.

CONCLUSION

In conclusion, we have unveiled the structural and biochemical basis of a unique enzymatic THF formation catalyzed by a cytochrome P450 monooxygenase. Through elucidation of four AurH variant crystal structures, which represent the first structures within the CYP151A family, inhibition studies, modeling, and site-directed mutagenesis, we have identified key residues that are required for the regio- and stereoselective hydroxylation and subsequent THF ring formation. On the basis of our results, we developed a model in which the hydroxylated intermediate changes its conformation in the binding site due to a sterical switch of the enzyme, thus allowing the second oxygenation-heterocyclization step. Furthermore, we engineered mutants with diverging regiospecificity and function. The isolation and full structure elucidation of three new aureothin analogues produced by the AurH variants revealed that these mutants favor C-9a oxygenation and produce hydroxyl, aldehyde, and carboxylate moieties. Overall, AurH represents a fascinating example of a fine-tuned, multifunctional biocatalyst of high synthetic value. Thus, our work not only provides new insights into finesse of enzyme-mediated oxygenation reactions, but also sets the ground for future enzyme engineering in the field of synthetically useful biotransformations. Since related five- and six-membered *O*-heterocycles are integral components of many bioactive polyketides,[43] we believe that the dual function of AurH-type oxygenases is more widespread in nature.

EXPERIMENTAL SECTION

Structure Determination, Refinement, and Substrate Modeling. Data collection was carried out with five protein crystals (Table 1). One crystal of nterm-AurH-II was used for phase determination by performing a MAD experiment. Freshly prepared crystals were used for collecting the data sets of nterm-AurH-I, nterm-AurH-II, Ancymidol:AurH, and wt-AurH. Data reduction was performed using XDS and XSCALE.[44] The iron position was located using SHELXD[45] and used for phasing and density modification as implemented in SHARP/autoSHARP.[46] The final experimental electron density map was of decent quality (figure of merit 0.408) and allowed automatic chain tracing performed by ARP/wARP,[47] which resulted in a partial model of 367 residues. This model was transferred to the high resolution data set using rigid body refinement of REFMAC5.[48] Several cycles of manual building with COOT[49] and refinement with REFMAC5 completed the model. Water molecules were placed using ARP/wARP and checked manually with COOT. The final refinement steps involved TLS group refinement. Therefore, the structure was divided into eight TLS groups yielding a model of excellent quality (Table 1). The chloride ions located in nterm-AurH-II were inserted after examining the chemical environment and the anomalous electron density [F+(lrem) − F-(lrem)] of the low remote data set calculated by SFTOOLS[48] and FFT.[48] Phasing for Ancy:AurH was done by molecular replacement procedure using rigid body refinement of REFMAC5.[48] The phases for wt-AurH resulted from molecular replacement using PHASER.[48] Model bias of Ancy:AurH and wt-AurH were avoided by simulated annealing using PHENIX.[50] The following refinement procedure was similar to that described for nterm-AurH. Due to the lower amount of reflections, however, only up to two TLS groups per protomer were used for the final refinement steps. All structures were validated using WHATCHECK[48] and SFCHECK[48] (Table 2). Figures were generated using POVscript+[51] and POVRAY (www.povray.org).

Molecular Docking. The structures of wt-AurH, Ancy:AurH, and nterm-AurH-I served as templates for our docking calculations of the substrates **3** and **2** using AUTODOCK4.[29] When performing the docking calculations, all water molecules beside the distal water of the heme group were removed. Q91 was assigned as a flexible residue because it was observed that this residue adopts different conformations in Ancy:AurH and the unbound structures. All other amino acids remained as rigid.

For the substrates **2** and **3** only the bonds between C9−C8, C8−C7, C7−C6, and the ether group of the pyrone ring system were allowed to rotate during docking calculations while the conjugated system remained rigid. The grid box covered the complete active center, and docking was performed with 25 cycles using Lamarckian genetic algorithm (LGA). The docked models were visualized and analyzed for structural and chemical sense.

Accession Codes. The structure of nterm-AurH-I, nterm-AurH-II, and wt-AurH and the structure of AurH in complex with ancymidol have been deposited in the PDB database under accession codes 3P3L, 3P3O, 3P3X, and 3P3Z, respectively.

Mutagenesis and Activity Assays. For mutational analyses, an *in vivo*-approach was chosen. The *aurH* gene was cloned into an *E. coli*−*Streptomyces* shuttle vector downstream of the constitutively active *ermE* promoter from the erythromycin biosynthesis gene cluster. Mutations were introduced into the *aurH* sequence with the QuikChange XL II Kit (Stratagene) according to the manufacturer's instructions (see Supporting Information Table S3 for primer sequences). Correct clones were identified by sequencing and were transferred into wild type *S. albus*. Aliquots of spore suspension (10 μL) were used to inoculate seed cultures of J medium (10 mL) supplemented with thiostrepton (5 mg L^{-1}). After incubation at 30 °C with orbital shaking at 160 rpm for 24 h, 3 mL of the seed culture was used to inoculate M10 medium (30 mL) containing thiostrepton (5 mg L^{-1}). Cultivation was continued for another day before deoxyaureothin (**3**) (0.5 mg, 43.5 μmol L^{-1} final concentration) was added to each culture. After distinct time intervals of ongoing cultivation, aliquots (5 mL) were taken and extracted once with ethyl acetate (5 mL each). The organic phases were collected and evaporated under reduced pressure. The dried extracts were redissolved in methanol (1 mL), and aliquots (20 μL) were subjected to HPLC−UV−MS measurements on an ET 250/4 Nucleosil 120−5 C8 column from Macherey-Nagel. Separation was achieved by elution at 1 mL min^{-1} in a gradient (20 min) from 20% to 98% acetonitrile in water (0.1% formic acid). MS detection was carried out in positive mode.

Production, Purification, and Structure Elucidation of Novel Aureothin Derivatives. For production of suitable amounts of the new deoxyaureothin derivatives, *S. albus* strains were generated that harbor an integrative plasmid with genes coding for deoxyaureothin (**3**) biosynthesis (i.e., aureothin biosynthesis gene cluster lacking the *aurH* gene)[13] and a plasmid coding for AurH mutant F89W. A seed culture of J medium (10 mL), supplemented with thiostrepton (5 mg L^{-1}) and apramycin (30 mg L^{-1}), was inoculated with a spore suspension (10 μL) of the *S. albus* mutant strain and incubated at 30 °C with orbital shaking at 200 rpm. After 24 h, a larger seed culture of identical medium (1 L) was inoculated with the first seed culture, and incubation was continued at 28 °C/120 rpm for another two days. M10 medium [14 L, supplemented with thiostrepton (5 mg L^{-1}) and apramycin (30 mg L^{-1})] was inoculated using the 1 L seed culture in a stainless steel fermenter. Cultivation was carried out for six days at 28 °C and continuous stirring at 400 rpm without pH adjustment.

The cultivation broth was separated from cellular material by centrifugation and extracted twice with equal volumes of ethyl acetate. The combined organic phases were dried over sodium sulfate and concentrated under reduced pressure. The residue was dissolved in chloroform and subjected to open column chromatography on silica gel using chloroform as the initial mobile phase. Several fractions containing deoxyaureothin derivatives **4**−**6** were obtained using a chloroform−methanol gradient for elution. After further purification on Sephadex LH-20 (methanol), the final separation of **5** was achieved by preparative HPLC (Nucleosil C18) using a water (0.1% trifluoracetic acid)/acetonitrile gradient (up to 83% acetonitrile), yielding 20 mg of deoxyaureothin-9a-aldehyde (**5**).

Fractions containing **4** were purified via preparative HPLC (Nucleosil C18) using a gradient from 0.1% aqueous $(NH_4)HCO_3$ to 83% acetonitrile. Concentration under reduced pressure afforded 3.6 mg of 9a-hydroxydeoxyaureothin (**4**).

The last fraction of the silica gel chromatography was concentrated, and the residue was dissolved in ethyl acetate (250 mL) and extracted three times with aq Tris (100 mL, 100 mM, pH 8.0). The combined aqueous phases were washed three times with ethyl acetate (50 mL each), followed by acidification with aq NaH_2PO_4 (100 mL, 1 M, pH 2.0). The turbid solution was extracted four times with ethyl acetate (100 mL each). The combined organic phases were dried over sodium sulfate and concentrated under reduced pressure to yield deoxyaureothin-9-carboxylic acid (**6**) as a mixture of *E*/*Z*-isomers. The isomers were dissolved in a 1:3 mixture of DMSO and acetonitrile and separated by preparative HPLC (Nucleosil C18) with isocratic elution (42% acetonitrile in water containing 0.1% TFA). Re-extraction with ethyl acetate afforded 17 mg of (9*Z*,11*E*)-deoxyaureothin-9-carboxylic acid (**6**, referred to as the genuine deoxyaureothin-9-carboxylic acid), and 20 mg of (9*Z*,11*Z*)-deoxyaureothin-9-carboxylic acid, resulting from light-induced isomerization.

*9a-Hydroxydeoxyaureothin (**4**).* Yellow, amorphous solid (3.6 mg). ^{1}H NMR (500 MHz, $CDCl_3$): 8.16 (d, *J* = 8.7 Hz, 2H, H-15/17), 7.33 (d, *J* = 8.6 Hz, 2H, H-14/18), 6.34 (s, 1H, H-12), 6.14 (s, 1H, H-10), 4.22 (s, 2H, H-9a), 3.77 (s, 3H, H-2a), 2.78 (t, *J* = 7.5 Hz, 2H, H-7), 2.68 (t, *J* = 7.5 Hz, 2H, H-8), 1.92 (s, 3H, H-11a), 1.88 (s, 3H, H-5a), 1.78 (s, 3H, H-3a). ^{13}C NMR (125 MHz, $CDCl_3$): 179.0 (C-4), 160.3 (C-2), 155.5 (C-6), 144.3 (C-16), 142.2 (C-13), 137.6 (C-9), 136.9 (C-11), 129.6 (C-10), 127.7 (C-14/18), 125.4 (C-12), 121.8 (C-15/17), 116.8 (C-5), 97.7 (C-3), 64.9 (C-9a), 53.3 (C-2a), 28.1 (C-7), 24.5 (C-8), 17.2 (C-11a), 8.2 (C-5a), 5.0 (C-3a). FT-IR (solid film): ν 3422 (OH), 2925 (CH_3), 2857 (O−CH_3), 1662 (C═O), 1581 (C═C), 1512 (NO_2), 1337 (NO_2), 855 (vicinal ar H) cm^{-1}. UV(MeOH) λ_{max} (lg ε): 247.5 (4.12), 341 (4.03) nm. (+)-ESI-MS *m*/*z* 422 $[M + Na]^+$, *m*/*z* 400 $[M + H]^+$, MS^n *m*/*z* 168, *m*/*z* 152. HRESI-MS *m*/*z* $[M + H]^+$ calcd for $C_{22}H_{26}NO_6$ 400.1755; found 400.1743.

*Deoxyaureothin-9a-aldehyde (**5**).* Yellow, amorphous solid (20 mg). ^{1}H NMR (600 MHz, $CDCl_3$): 9.48 (s, 1H, H-9a), 8.24 (d, *J* = 8.6 Hz, 2H, H-15/17), 7.42 (d, *J* = 8.6 Hz, 2H, H-14/18), 6.95 (s, 1H, H-10), 6.75 (s, 1H, H-12), 3.86 (s, 3H, H-2a), 2.86 (t, *J* = 7.4 Hz, 2H, H-8), 2.76 (t, *J* = 7.4 Hz, 2H, H-7), 2.13 (s, 3H, H-11a), 1.88 (s, 3H, H-5a), 1.79 (s, 3H, H-3a). ^{13}C NMR (125 MHz, $CDCl_3$): 194.9 (C-9a), 180.7 (C-4), 162.1 (C-2), 156.7 (C-6), 154.5 (C-10), 146.8 (C-16), 142.4 (C-13), 140.3 (C-9), 136.8 (C-11), 134.3 (C-12), 129.9 (C-14/18), 123.6 (C-15/17), 118.9 (C-5), 99.4 (C-3), 55.2 (C-2a), 29.8 (C-7), 22.6 (C-8), 17.7 (C-11a), 10.0 (C-5a), 6.8 (C-3a). FT-IR (solid film): ν 2927 (CH_3), 2866 (O−CH_3), 1663 (C═O), 1592 (C═C), 1518 (NO_2), 1341 (NO_2), 855 (vicinal ar H) cm^{-1}. UV (MeOH) λ_{max} (lg ε): 259 (4.30), 333.5 (4.28) nm. (+)-ESI-MS *m*/*z* 420 $[M + Na]^+$, *m*/*z* 398 $[M + H]^+$. MS^n *m*/*z* 168, *m*/*z* 153. HRESI-MS *m*/*z* $[M + H]^+$ calcd for $C_{22}H_{24}NO_6$ 398.1598; found 398.1596.

*Deoxyaureothin-9-carboxylic Acid (**6**).* Yellow, amorphous solid (17 mg). ^{1}H NMR (300 MHz, DMSO-d_6): 12.9 (br,H-9a), 8.20 (d, *J* = 8.9 Hz, 2H, H-15/17), 7.55 (d, *J* = 8.8 Hz, 2H, H-14/18), 6.58 (s, 1H, H-10), 6.33 (s, 1H, H-12), 3.97 (s, 3H, H-2a), 2.81 (t, *J* = 7.1 Hz, 2H, H-7), 2.64 (t, *J* = 7.1 Hz, 2H, H-8), 1.97 (d, *J* = 1.0 Hz, 3H, H-11a), 1.81 (s, 3H, H-5a), 1.68 (s, 3H, H-3a). ^{13}C NMR (125 MHz, DMSO-d_6): 179.3 (C-4), 170.3 (C-9a), 161.8 (C-2), 157.1 (C-6), 145.7 (C-16), 143.7 (C-13), 138.3 (C-11), 136.5 (C-10), 133.6 (C-9), 130.1 (C-14/18), 129.5 (C-12), 123.5 (C-15/17), 117.8 (C-5), 97.5 (C-3), 55.7 (C-2a), 32.4 (C-8), 29.5 (C-7), 16.8 (C-11a), 9.6 (C-5a), 6.9 (C-3a). FT-IR (solid film): ν 2927 (CH_3), 2874 (O−CH_3), 2521 (OH), 1660 (C═O), 1590 (C═C), 1514 (NO_2), 1338 (NO_2), 856 (vicinal ar H) cm^{-1}. UV (MeOH) λ_{max}: 253, 339 nm. (+)-ESI-MS *m*/*z* 436 $[M + Na]^+$, *m*/*z* 414 $[M + H]^+$. MS^n *m*/*z* 168, *m*/*z* 153. HRESI-MS *m*/*z* $[M + H]^+$ calcd for $C_{22}H_{24}NO_7$ 414.1547; found 414.1542.

■ ASSOCIATED CONTENT

Supporting Information. Sequence alignment of AurH homologues, primer sequences for mutagenesis, additional information about the activity of mutants, spectra of new aureothin derivatives. This material is available free of charge via the Internet at http://pubs.acs.org.

■ AUTHOR INFORMATION

Corresponding Author

georg.zocher@uni-tuebingen.de (G.Z., for stuctural biology correspondence); Christian.Hertweck@hki-jena.de (C.H., for biochemistry/chemistry correspondence)

Author Contributions

#These authors contributed equally.

■ ACKNOWLEDGMENT

We gratefully acknowledge the BESSY beamlines BL14.1 and BL14.2 for offering beamtime. We thank Prof. Dr. Udo Heinemann for the opportunity to work in his lab and Dr. Yvette Roske for the introduction to the hydra-II crystallization robot. We also thank A. Perner for MS and HPLC/MS measurements, and F. Rhein for NMR measurements. Financial support by the DFG is gratefully acknowledged.

■ REFERENCES

(1) Nelson, D. R. *Arch. Biochem. Biophys.* **1999**, *369*, 1–10.
(2) Guengerich, F. P. *J. Biochem. Mol. Toxicol.* **2007**, *21*, 163–8.
(3) Isin, E. M.; Guengerich, F. P. *Biochim. Biophys. Acta* **2007**, *1770*, 314–29.
(4) Takahashi, S.; Yeo, Y. S.; Zhao, Y.; O'Maille, P. E.; Greenhagen, B. T.; Noel, J. P.; Coates, R. M.; Chappell, J. *J. Biol. Chem.* **2007**, *282*, 31744–54.
(5) Glieder, A.; Farinas, E. T.; Arnold, F. H. *Nat. Biotechnol.* **2002**, *20*, 1135–9.
(6) Bistolas, N.; Wollenberger, U.; Jung, C.; Scheller, F. W. *Biosens. Bioelectron.* **2005**, *20*, 2408–23.
(7) Müller, M.; He, J.; Hertweck, C. *ChemBioChem* **2006**, *7*, 37–39.
(8) He, J.; Hertweck, C. *Chem. Biol.* **2003**, *10*, 1225–1232.
(9) Werneburg, M.; Busch, B.; He, J.; Richter, M. E.; Xiang, L.; Moore, B. S.; Roth, M.; Dahse, H. M.; Hertweck, C. *J. Am. Chem. Soc.* **2010**, *132*, 10407–13.
(10) Richter, M. E.; Traitcheva, N.; Knupfer, U.; Hertweck, C. *Angew. Chem., Int. Ed.* **2008**, *47*, 8872–5.
(11) Werneburg, M.; Hertweck, C. *ChemBioChem* **2008**, *9*, 2064–6.
(12) Traitcheva, N.; Jenke-Kodama, H.; He, J.; Dittmann, E.; Hertweck, C. *ChemBioChem* **2007**, *8*, 1841–9.
(13) He, J.; Muller, M.; Hertweck, C. *J. Am. Chem. Soc.* **2004**, *126*, 16742–3.
(14) Fischer, M.; Knoll, M.; Sirim, D.; Wagner, F.; Funke, S.; Pleiss, J. *Bioinformatics* **2007**, *23*, 2015–7.
(15) Ralston, L.; Kwon, S. T.; Schoenbeck, M.; Ralston, J.; Schenk, D. J.; Coates, R. M.; Chappell, J. *Arch. Biochem. Biophys.* **2001**, *393*, 222–35.
(16) Holm, L.; Sander, C. *J. Mol. Biol.* **1993**, *233*, 123–38.
(17) Sherman, D. H.; Li, S.; Yermalitskaya, L. V.; Kim, Y.; Smith, J. A.; Waterman, M. R.; Podust, L. M. *J. Biol. Chem.* **2006**, *281*, 26289–97.
(18) Sugimoto, H.; Shinkyo, R.; Hayashi, K.; Yoneda, S.; Yamada, M.; Kamakura, M.; Ikushiro, S.; Shiro, Y.; Sakaki, T. *Biochemistry* **2008**, *47*, 4017–27.
(19) Cryle, M. J.; Schlichting, I. *Proc. Natl. Acad. Sci. U.S.A.* **2008**, *105*, 15696–701.
(20) McCoy, J. G.; Johnson, H. D.; Singh, S.; Bingman, C. A.; Lei, I. K.; Thorson, J. S.; Phillips, G. N., Jr. *Proteins* **2009**, *74*, 50–60.
(21) Makino, M.; Sugimoto, H.; Shiro, Y.; Asamizu, S.; Onaka, H.; Nagano, S. *Proc. Natl. Acad. Sci. U.S.A.* **2007**, *104*, 11591–6.
(22) Nagano, S.; Li, H.; Shimizu, H.; Nishida, C.; Ogura, H.; Ortiz de Montellano, P. R.; Poulos, T. L. *J. Biol. Chem.* **2003**, *278*, 44886–93.
(23) Gotoh, O. *J. Biol. Chem.* **1992**, *267*, 83–90.
(24) Lee, D. S.; Yamada, A.; Sugimoto, H.; Matsunaga, I.; Ogura, H.; Ichihara, K.; Adachi, S.; Park, S. Y.; Shiro, Y. *J. Biol. Chem.* **2003**, *278*, 9761–7.
(25) Cojocaru, V.; Winn, P. J.; Wade, R. C. *Biochim. Biophys. Acta* **2007**, *1770*, 390–401.
(26) Nagano, S.; Poulos, T. L. *J. Biol. Chem.* **2005**, *280*, 31659–63.
(27) Schlichting, I.; Berendzen, J.; Chu, K.; Stock, A. M.; Maves, S. A.; Benson, D. E.; Sweet, R. M.; Ringe, D.; Petsko, G. A.; Sligar, S. G. *Science* **2000**, *287*, 1615–22.
(28) Cupp-Vickery, J. R.; Garcia, C.; Hofacre, A.; McGee-Estrada, K. *J. Mol. Biol.* **2001**, *311*, 101–10.
(29) Morris, G. M.; Huey, R.; Lindstrom, W.; Sanner, M. F.; Belew, R. K.; Goodsell, D. S.; Olson, A. J. *J. Comput. Chem.* **2009**, *30*, 2785–91.
(30) Eswar, N.; Eramian, D.; Webb, B.; Shen, M. Y.; Sali, A. *Methods Mol. Biol.* **2008**, *426*, 145.
(31) Yano, J. K.; Hsu, M. H.; Griffin, K. J.; Stout, C. D.; Johnson, E. F. *Nat. Struct. Mol. Biol.* **2005**, *12*, 822–3.
(32) Li, S.; Ouellet, H.; Sherman, D. H.; Podust, L. M. *J. Biol. Chem.* **2009**, *284*, 5723–30.
(33) Sansen, S.; Hsu, M. H.; Stout, C. D.; Johnson, E. F. *Arch. Biochem. Biophys.* **2007**, *464*, 197–206.
(34) Dietrich, M.; Do, T. A.; Schmid, R. D.; Pleiss, J.; Urlacher, V. B. *J. Biotechnol.* **2009**, *139*, 115–7.
(35) Whitehouse, C. J.; Bell, S. G.; Wong, L. L. *Chemistry* **2008**, *14*, 10905–8.
(36) Whitehouse, C. J.; Bell, S. G.; Yang, W.; Yorke, J. A.; Blanford, C. F.; Strong, A. J.; Morse, E. J.; Bartlam, M.; Rao, Z.; Wong, L. L. *ChemBioChem* **2009**, *10*, 1654–6.
(37) Lentz, O.; Feenstra, A.; Habicher, T.; Hauer, B.; Schmid, R. D.; Urlacher, V. B. *ChemBioChem* **2006**, *7*, 345–50.
(38) Helliwell, C. A.; Poole, A.; Peacock, W. J.; Dennis, E. S. *Plant. Physiol.* **1999**, *119*, 507–10.
(39) Rojas, M. C.; Hedden, P.; Gaskin, P.; Tudzynski, B. *Proc. Natl. Acad. Sci. U.S.A.* **2001**, *98*, 5838–43.
(40) Ro, D. K.; Arimura, G.; Lau, S. Y.; Piers, E.; Bohlmann, J. *Proc. Natl. Acad. Sci. U.S.A.* **2005**, *102*, 8060–5.
(41) Teoh, K. H.; Polichuk, D. R.; Reed, D. W.; Nowak, G.; Covello, P. S. *FEBS Lett.* **2006**, *580*, 1411–6.
(42) Olano, C.; Wilkinson, B.; Sanchez, C.; Moss, S. J.; Sheridan, R.; Math, V.; Weston, A. J.; Brana, A. F.; Martin, C. J.; Oliynyk, M.; Mendez, C.; Leadlay, P. F.; Salas, J. A. *Chem. Biol.* **2004**, *11*, 87–97.
(43) Hertweck, C. *Angew. Chem., Int. Ed.* **2009**, *48*, 4688–4716.
(44) Kabsch, W. *J. Appl. Crystallogr.* **1993**, *26*, 795–800.
(45) Sheldrick, G. M. *Acta Crystallogr., Sect. D* **2010**, *66*, 479–485.
(46) Bricogne, G. *Methods Enzymol.* **1997**, *277*, 14–8.
(47) Langer, G.; Cohen, S. X.; Lamzin, V. S.; Perrakis, A. *Nat. Protoc.* **2008**, *3*, 1171–9.
(48) Collaborative Computational Project, Number 4. *Acta Crystallogr., Sect. D: Biol. Crystallogr.* **1994**, *50*, 760-3.
(49) Emsley, P.; Cowtan, K. *Acta Crystallogr., Sect. D: Biol. Crystallogr.* **2004**, *60*, 2126–32.
(50) Adams, P. D.; Afonine, P. V.; Bunkoczi, G.; Chen, V. B.; Davis, I. W.; Echols, N.; Headd, J. J.; Hung, L. W.; Kapral, G. J.; Grosse-Kunstleve, R. W.; McCoy, A. J.; Moriarty, N. W.; Oeffner, R.; Read, R. J.; Richardson, D. C.; Richardson, J. S.; Terwilliger, T. C.; Zwart, P. H. *Acta Crystallogr. Sect. D: Biol. Crystallogr.* **2010**, *66*, 213–21.
(51) Fenn, T. D.; Ringe, D.; Petsko, G. A. *J. Appl. Crystallogr.* **2003**, *36*, 944–947.